Competition between pattern recall and sequence processing in a neural network storing correlated patterns

1995 J. Phys. A: Math. Gen. 28 3421

(http://iopscience.iop.org/0305-4470/28/12/016)

J. Phys. A: Math. Gen. 28 (1995) 3421–3437. Printed in the UK

Competition between pattern recall and sequence processing in a neural network storing correlated patterns

W Whyte, D Sherrington and A C C Coolen
Theoretical Physics, Department of Physics, 1 Keble Road, Oxford OX1 3NP, UK

Received 28 September 1994, in final form 16 March 1995

Abstract. We investigate the effects on a network that stores a sequence of patterns without time delays of introducing patterns that are correlated in a way that depends only on their separation from each other in the sequence. We demonstrate that with a carefully chosen form for the synaptic matrix, the introduction of these correlations can, under certain circumstances, aid the recall of the individual patterns while still preserving the limit-cycle behaviour of the net.

1. Introduction

Models of neural networks have been a fruitful source of insight into the possible structure of associative memories. Two of the most common simplifications have been to assume symmetric, instantaneous synaptic interactions between the neurons, and to use Ising neurons whose state can only take the values $\{-1, 1\}$ (see, for example, Hopfield [1], Amit *et al* [2]). An attractor neural network with a symmetric synaptic matrix, operating under the commonly used dynamic laws, will always end up in either a fixed point (under sequential or parallel dynamics) or a period-2 limit cycle (under parallel dynamics). Clearly, while these models are useful for studying static memories, they need to be adapted to make possible a study of dynamic memories, or memories with a more complicated structure.

Two main approaches have emerged to the problem of trying to store memories that change over time. One is to assume a distribution of transmission delays in the synaptic interactions (as was done by Kleinfeld [3] and Sompolinsky and Kanter [4]). By using a model that employed a temporal symmetry of the synaptic matrix, Herz *et al* [5] have been able to derive many useful results, such as the storage capacity and the phase diagram of their Hebb-like model. The other approach, which we follow here, is to preserve the concept of interactions being instantaneous and to see what kinds of behaviour can be obtained using only the asymmetry of the synaptic matrix. Buhmann and Schulten [6] showed that it was possible to obtain cyclic behaviour in a neural network at a finite operating temperature, and Nakamura and Nishimori [7] performed a detailed analysis on a sparse-coded network which found that this cycling behaviour persisted even at zero temperature. More recently, Coolen and Sherrington [8] have investigated competition between a sequence-processing term and a pattern-storing term in a neural network without transmission delays or sparse coding.

In this paper, we study the effects of introducing correlations between patterns to a network that features competition between pattern storage and sequence processing without using transmission delays. This network displays limit-cycle behaviour in a large region of the phase diagram. From a practical point of view, the most interesting and useful

0305-4470/95/123421+17$19.50

behaviour of the network is when it is in a stable limit cycle with the individual pattern overlaps taking a wide range of values. For reasons to be given, we expect correlations to exist between patterns in a sequence in a biological network; we are therefore strongly motivated to see if their effects will be constructive or destructive on recall of the sequence as a whole.

The first of the networks that we study is very similar to that analysed (without correlations) by Coolen and Sherrington [8], henceforth referred to as CS. Here we show that the effect of the correlations, in combination with the competing aspects of the dynamics, is to tend to 'smear out' the network into a state of equal overlap with all the patterns. The second network is more reminiscent of those in [6, 7]. Here, when we introduce an extra term into the synaptic matrix designed to suppress this symmetric mixture state, we discover that increasing the correlations will increase the range of values that the individual pattern overlaps take and improve the robustness of the sequence processing behaviour. This improvement is greatest for non-zero temperature and for a network intermediate between the two extremes of pure sequence processing and pure Hebbian pattern storage.

We will be looking at patterns whose total 'magnetization' is zero, but which are positively correlated with the patterns that come close to them in the stored sequence. We take the correlation to decrease with the separation of the two patterns in the sequence, and to only depend on that separation. This form of correlation is inspired from several different sources. It is intuitively appealing that the patterns in a remembered sequence will be correlated in a way that depends on their separation, if only because, since things in the real world change continuously, one stimulus will inevitably have some similarity to the ones immediately before and after it. Secondly, experiments on monkeys performed by Miyashita *et al* [9–11] have demonstrated that if they are presented with a set sequence of stimuli many times, then subsequently presenting them with a stimulus from the sequence will result in their recalling not just that stimulus, but its neighbours in the sequence. This phenomenon was modelled by Griniasty *et al* [12] assuming that the stored patterns corresponding to the stimuli were uncorrelated but that the neural interactions modify themselves so as to recall the patterns that have become associated with the presented one. Here, we are inspired by this result to consider the case in which the stored patterns are correlated. Finally, many of the results derived in CS only depended on the matrix of correlations of the patterns being Toeplitz. This paper can therefore be regarded in part as a generalization of this previous work.

This paper is organized as follows. In section 2 we define the form of the synaptic matrix and of the correlations. In section 3 we investigate the effects of correlations on the synaptic matrix of CS, and show that the effect of increasing correlations is to decrease both the area of the phase diagram in which limit-cycle behaviour will take place and the ability of the network to distinguish between patterns. In section 4 we look at a slightly different synaptic matrix, and show that in this case increasing the correlations improves the quality of the limit-cycle behaviour in certain circumstances.

2. Construction of the network and correlations

2.1. Synaptic matrix and dynamic laws

Our model is an Ising spin neural network of N spins $s_i \in \{-1, 1\}$, corresponding to neuron i being at rest or firing, respectively. We wish to study a system that has learned a given

set of patterns $\xi^\mu \in \{-1, 1\}^N$, $\mu = 1, \ldots, p$, via synapses

$$J_{ij} = \frac{1}{N} \sum_{\mu\rho=1}^{p} \xi_i^\mu A_{\mu\rho} \xi_j^\rho \,. \tag{1}$$

The quantities of interest are the macroscopic overlaps

$$q_\mu(\vec{s}) \equiv \frac{1}{N} \sum_{i=1}^{N} \xi_i^\mu s_i \qquad (\mu = 1 \ldots p) \tag{2}$$

whose evolution we wish to study under parallel (synchronous) dynamics and sequential (asynchronous) dynamics. In both these cases we take $p \ll \sqrt{N}$ as $N \to \infty$.

For the case of a parallel (Markov) process, all of the neurons are updated simultaneously following the rule $P[s_i(t+1)] = \frac{1}{2}(1 + s_i(t+1) \tanh[\beta \sum_j J_{ij} s_j(t)])$. The evolution in time of the q_μ's in the thermodynamic limit is governed by the set of coupled nonlinear mappings

$$\vec{q}_{t+1} = \langle \vec{\xi} \tanh[\beta \vec{\xi} \cdot \mathbf{A} \vec{q}_t] \rangle_{\vec{\xi}} \tag{3}$$

where the average is defined as

$$\langle \Phi(\vec{\xi}) \rangle_{\vec{\xi}} \equiv \sum_{\vec{\xi} \in \{-1,1\}^p} P(\vec{\xi}) \Phi(\vec{\xi}) \qquad \text{with} \qquad P(\vec{\xi}) \equiv \lim_{N\to\infty} \frac{1}{N} \sum_i \delta[\vec{\xi}_i - \vec{\xi}]$$

$$\vec{\xi}_i \equiv (\xi_i^1 \ldots \xi_i^p) \,. \tag{4}$$

Under sequential dynamics, the individual neurons are updated one at a time in a random order, according to the rule $P(s_i) = \frac{1}{2}(1 + s_i \tanh[\beta \sum_j J_{ij} s_j])$. If we take the duration of a single iteration to scale as $\frac{1}{N}$, then in the thermodynamic limit the behaviour of the macroscopic overlaps q_μ is governed by the set of coupled nonlinear differential equations [13]

$$\frac{\mathrm{d}}{\mathrm{d}t} \vec{q} = \langle \vec{\xi} \tanh[\beta \vec{\xi} \cdot \mathbf{A} \vec{q}] \rangle_{\vec{\xi}} - \vec{q} \,. \tag{5}$$

The fixed points of either dynamics will satisfy

$$q_\mu = \langle \xi_\mu \tanh[\beta \vec{\xi} \cdot \mathbf{A} \vec{q}] \rangle_{\vec{\xi}} \,. \tag{6}$$

The forms of $\mathbf{A}$ under investigation here are

$$\begin{aligned} &\text{(i)} && A_{\mu\rho} \equiv \nu \delta_{\mu\rho} + (1 - \nu) S_{\mu\rho} \\ &\text{(ii)} && A_{\mu\rho} \equiv \nu \delta_{\mu\rho} + \tfrac{1}{2}\sqrt{1 - \nu^2}\, S_{\mu\rho} - \tfrac{1}{2}\sqrt{1 - \nu^2}\, S^+_{\mu\rho} \end{aligned} \tag{7}$$

where $S_{\mu\rho} \equiv \delta_{\mu,\rho+1}$ $(\mu : \mathrm{mod}\, p)$.

The parameter $\nu \in [0, 1]$ allows us to interpolate smoothly between the simple Hopfield model ($\nu = 1$) and sequence processing models ($\nu = 0$). The forms of the coefficients of $\mathbf{S}$ and $\mathbf{S}^+$ are chosen to obtain a value for the critical temperature for the existence of non-trivial fixed-point solutions that is independent of the value of ν. The effect of the first form of $\mathbf{A}$ on a system in a pure state μ will be to move it towards the state $\mu + 1$; the effect of the second form of $\mathbf{A}$ on the same system will be to move it towards a mixture of $\mu + 1$ and the inverse of $\mu - 1$. We therefore refer to the first $\mathbf{A}$ as 'forward-propagating' and to the second as 'double-propagating'; to distinguish them we call the latter $\mathbf{A}'$ hereafter.

For the forward-propagating case storing uncorrelated patterns and with parallel dynamics, CS obtained the phase diagram shown in figure 1, with similar behaviour for other p values. It contains six distinct regions (note that our notation differs from theirs).

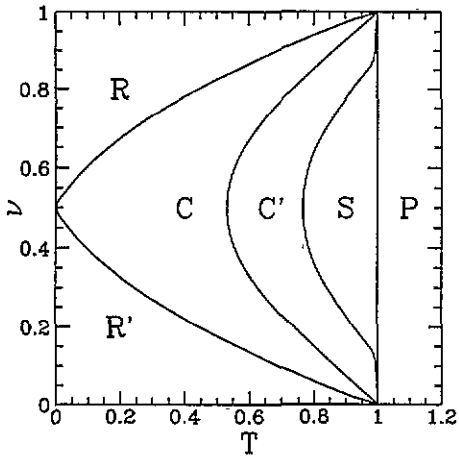

Figure 1. The phase diagram as determined by CS for $p = 10$. The labels refer to the phases described in the text.

- For $T > 1$ there is a paramagnetic phase (P), where the trivial fixed point will be the only fixed point of the dynamics.
- At $T_{ps} = 1 \geqslant T \geqslant T_{sc'}(\nu)$ there is a phase (S) in which the symmetric fixed point $\vec{q} = q^*(1, 1, 1, \ldots, 1)$ is the only attractor of the dynamics.
- At $T_{sc'}(\nu) \geqslant T \geqslant T_{cr}(\nu)$ the system exhibits limit-cycle behaviour, whose period depends on the value of ν. There are two regions within this temperature range, C and C'; within the region C' the symmetric fixed-point solution is also stable, whereas within C it is unstable. Their boundary is $T_{c'c}(\nu)$.
- For $T < T_{cr}(\nu)$ the system is in a 'retrieval' phase (R), in which there are stable non-symmetric fixed points and recall of individual patterns is possible.
- There is also a corresponding phase R' ($T < T_{cr'}$) in which the system displays limit-cycle behaviour with period p, independent of the value of ν.

Each of the critical temperature lines is symmetric under $\nu \to 1 - \nu$.

We might expect that the structure of the phase diagram for parallel dynamics with the matrix **A** and correlated patterns will be qualitatively the same as the structure of this phase diagram, but with altered parameters. In the case of the matrix **A'** it is more difficult to predict the detailed structure of the phase diagram *a priori*. We would expect the phases P, S, C and R to be observable. However, we would not expect to see an R' phase, since this phase arises as a result of the symmetry between ν and $1 - \nu$ under parallel dynamics for the matrix **A**, and this symmetry does not exist for **A'**. These expectations are, in fact, borne out.

2.2. *Pattern distribution and correlation*

In this paper we take $\langle \xi^\mu \rangle = 0$, and define the correlation matrix $C_{\mu\nu} \equiv \langle \xi^\mu \xi^\nu \rangle$. The patterns are not spatially correlated within themselves or biased; the correlations only enter as a relationship between the bits of different patterns on the same site i. We note that $C_{\mu\nu}$ is symmetric by definition, and require it to have the following additional properties:

(i) $C_{\rho\lambda} \equiv C_\Delta$, where $\Delta \equiv |\rho - \lambda|$ (**C** is translation-invariant in the space of patterns). **C** will therefore commute with both **A** and **A'**.

(ii) $C_{\rho\lambda}$ is positive in all its entries.

(iii) $C_{\rho\lambda}$ decreases monotonically from $C_{\rho\rho}$ ($\equiv 1$) to $C_{\rho,\rho+p/2}$, and thereafter (by the symmetry requirement) increases monotonically from $C_{\rho,\rho+p/2}$ to $C_{\rho,\rho-1}$.

When performing numerical simulations, and in order to have a single-parameter characterization of the whole distribution, we will assume that the probability distribution $P(\vec{\xi})$ is of a form corresponding to the thermal distribution of a periodic p-site one-dimensional nearest-neighbour Ising ferromagnet,

$$P(\vec{\xi}) \sim \mathrm{e}^{J(\sum_{\nu=1}^{p-1} \xi_\nu \xi_{\nu+1} + \xi_p \xi_1)} . \tag{8}$$

This gives a correlation matrix of the form

$$C_\Delta = \frac{t_J^\Delta + t_J^{p-\Delta}}{1 + t_J^p} \tag{9}$$

with $t_J \equiv \tanh(J) \in [-1, 1]$, which satisfies the conditions above, provided that $J \geqslant 0$.

The parameter we will generally use as a measure of the correlations is $c \equiv \langle \xi_\mu \xi_{\mu+1} \rangle_{\vec{\xi}}$, the correlation between nearest neighbours.

2.3. *Eigenvectors and eigenvalues*

As in CS, we define a set of vectors $\{|n\rangle\}$ which form an eigenbasis in p-dimensional space for the matrices **A**, **S** and **C**:

$$|n\rangle \equiv (\hat{e}_1^n, \ldots, \hat{e}_p^n) \qquad n = 0, \ldots, p-1 \qquad \hat{e}_\lambda^n \equiv \frac{1}{\sqrt{p}} \mathrm{e}^{2\pi \mathrm{i} n\lambda/p} . \tag{10}$$

These have the following properties:

$$\begin{aligned} &\langle n|m\rangle = \delta_{nm} \qquad \mathbf{S}|n\rangle = \mathrm{e}^{-2\pi \mathrm{i} n/p}|n\rangle \equiv s_n|n\rangle \qquad \mathbf{A}|n\rangle \equiv a_n|n\rangle \\ &\mathbf{C}|n\rangle \equiv c_n|n\rangle \qquad c_n = \sum_{\lambda=0}^{p-1} \cos(2\pi n\lambda/p) C_{1,\lambda+1} . \end{aligned} \tag{11}$$

For both the **A**'s to be studied here, a_n is real only if $n = 0$ or (if p is even) $n = p/2$. With regard to **C**, we note that $c_n = c_{p-n}$, that c_n is always real, and that $\max_n c_n = c_0 = \sum_\lambda C_{\rho\lambda}$. When p is even, $\min_n C_n = c_{p/2} = \sum_\lambda (-1)^\lambda C_{\rho\lambda}$.

We can write the symmetric fixed point in this basis as

$$\vec{q} \equiv \vec{q}^{\,+} = q^+|0\rangle . \tag{12}$$

If we take the correlations to be of the Ising ferromagnet type, the c_ns become

$$c_n = \frac{(1 - t_J^p)(1 - {t_J}^2)}{(1 + t_J^p)\left(1 + {t_J}^2 - 2t_J \cos\left[\frac{2n\pi}{p}\right]\right)} . \tag{13}$$

In this case, it can be seen that the eigenvalues c_n also obey the condition $c_{n+1} < c_n$, so long as $t_J > 0$ and $n + 1 < p/2$. In the limit $t_J \to 0$, $c_n \to 1 \,\forall n$; in the limit $t_J \to 1$, $c_0 \to p$ and $c_n \to 0$, $\forall n \neq 0$.

Eigenvalues of any matrix with respect to the basis $\{|n\rangle\}$ are denoted by latin subscripts; references to a particular pattern are denoted by Greek subscripts. We will also find it useful to define

$$\vec{\xi}|n\rangle \equiv x_n . \tag{14}$$

3. The forward-propagating A-matrix

In this section we take

$$A_{\mu\rho} \equiv \nu\delta_{\mu\rho} + (1-\nu)S_{\mu\rho} \tag{15}$$

so

$$\mathbf{A}|n\rangle = a_n|n\rangle = \left[\nu + (1-\nu)\mathrm{e}^{-2\pi \mathrm{i}n/p}\right]|n\rangle\,. \tag{16}$$

This is the case described for uncorrelated patterns by CS. For $p = 2$, this produces a symmetric synaptic matrix which may be analysed completely. We then perform as much analysis as possible on the $p > 2$ case, and follow this up with numerical simulations for $p = 10$.

3.1. The toy problem: the symmetric case $p = 2$

For $p = 2$, the probability distribution has the simple form

$$P[\xi^1, \xi^2] = \tfrac{1}{4}(1 + \xi^1\xi^2 c)\,. \tag{17}$$

If we introduce the variables $z^{\pm} \equiv q_1 \pm q_2$, the dynamic equations decouple, yielding the fixed-point equations

$$z^+_{fp} = (1+c)\tanh[\beta z^+_{fp}] \qquad z^-_{fp} = (1-c)\tanh[\beta(2\nu-1)z^-_{fp}] \tag{18}$$

which, in turn, imply the critical temperatures below which non-zero values of $z^{\pm}$ are possible:

$$T_c(z^+) = 1 + c \qquad T_c(z^-) = (1-c)(2\nu-1)\,. \tag{19}$$

We see that z^- will only be a non-zero fixed point if $\nu > 0.5$. However, if $\nu < 0.5$ and $T < T_c'(z^-) = (1-c)(1-2\nu)$, then under parallel dynamics z^- can oscillate between $\pm z^{-\prime}_{fp} = (1-c)\tanh[\beta(1-2\nu)z^{-\prime}_{fp}]$. We can thus identify four of the six phases from the general phase diagram:

- For $T > T_c(z^+) = (1+c)$ we are in the paramagnetic phase P.
- For $1 + c > T > (1-c)(|2\nu-1|)$, z^+ is non-zero and z^- is zero, and we are in the symmetric fixed-point phase S. There is no C phase.
- For $T < (1-c)(|2\nu-1|)$ we are in either R or R′, depending on whether ν is greater or less than 0.5, respectively.

The effect of increasing the correlation c for $p = 2$ is, therefore, to decrease the size of the regions P, R and R′. We would also expect to observe this at higher values of p. However, this toy model casts no light on the effect of increasing correlations on the relative sizes of regions S, C′ and C.

3.2. Analytic results for $p > 2$, parallel dynamics

We first attempt to locate the critical temperature T_{ps} for a transition from the paramagnetic phase to the symmetric fixed-point phase. An upper bound on this temperature is given by the critical temperature T_c for the existence of non-zero solutions of the fixed-point equation (6). Using the methods of CS, and the fact that $\max_n |a_n|$ and $\max_n c_n$ both occur at $n = 0$, we find that this temperature obeys

$$T \leqslant \tfrac{1}{2}\max_n\left[\langle n|\mathbf{C}|n\rangle + \langle n|\mathbf{A}^+\mathbf{C}\mathbf{A}|n\rangle\right] = \sum_{\Delta} C_{\Delta} = c_0\,. \tag{20}$$

The fact that this maximum occurs at $n = 0$ also indicates that the first type of non-trivial fixed point to become a solution of the dynamics is the symmetric fixed point, emphasizing that the temperature we are locating here is indeed T_{ps}.

A lower bound on T_{ps} can be obtained by stability and bifurcation analysis of the trivial fixed point. The condition for a fixed point $\vec{q}$ to bifurcate under parallel dynamics is

$$\det|\mathbf{1} - \beta\Gamma(\vec{q})\mathbf{A}| = 0 \qquad \text{where} \qquad \Gamma_{\rho\lambda} \equiv \langle \xi_\rho \xi_\lambda (1 - \tanh^2[\beta \vec{\xi}\mathbf{A} \cdot \vec{q}]) \rangle_{\vec{\xi}} \,. \tag{21}$$

The condition for local stability of a fixed point under parallel dynamics is

$$\max_{\vec{x}} \frac{\vec{x} \cdot \mathbf{A}^\dagger \Gamma^2(\vec{q}) \mathbf{A} \vec{x}}{\vec{x}^2} < T^2 \,. \tag{22}$$

Both these equations are to be solved simultaneously with the fixed-point equation (6).

For the trivial fixed point, $\Gamma(\vec{q}) = \Gamma(\vec{0}) = \mathbf{C}$. The bifurcation equation therefore becomes $\det|\mathbf{1} - \beta\mathbf{C}\mathbf{A}| = 0$, or

$$\exists \vec{y} : \mathbf{C}\mathbf{A}\vec{y} = T\vec{y} \,. \tag{23}$$

Because T is real, we require the left-hand side of this equation to be real. This means that $\vec{y} = |n\rangle$ where a_n is real. The only values of n that satisfy this are $n = 0$ and, if p is even, $n = p/2$. These two solutions have associated with them the critical temperatures

$$\begin{aligned} T_c(\vec{q} = q|0\rangle) &= \sum_\Delta C_\Delta \equiv c_0 \\ T_c(\vec{q} = q|p/2\rangle) &= (2\nu - 1) \sum_\Delta (-1)^\Delta C_\Delta \equiv (2\nu - 1) c_{p/2} < c_0 \,. \end{aligned} \tag{24}$$

On solving the stability equations for the trivial fixed point, we obtain, using the fact that $\Gamma(\vec{0}) = \mathbf{C}$, the condition

$$\max_n |a_n|^2 c_n < T^2 \quad \Rightarrow \quad T_c(\vec{q} = \vec{0} \text{ becomes unstable}) = c_0 \,. \tag{25}$$

We can conclude that at $T = c_0$ the trivial fixed point becomes unstable and bifurcates continuously to the symmetric fixed point. This fixes T_{ps}.

We now attempt to determine $T_{c'c}$. A stability analysis may be performed on the symmetric fixed point in the same way as on the trivial fixed point. In this case we obtain the following form for Γ:

$$\Gamma_{\rho\sigma}(\vec{q}^{\,+}) = \left\langle \xi_\rho \xi_\sigma \left(1 - \tanh^2 \left(\beta q^+ \frac{1}{\sqrt{p}} \sum_\nu \xi_\nu \right) \right) \right\rangle_{\vec{\xi}} \,. \tag{26}$$

It is evident that $\Gamma_{\rho\sigma}(\vec{q}^{\,+})$ will only depend on $|\rho - \sigma|$. It is also possible to express $\Gamma(\vec{q}^{\,+})$ in terms of the basis $|n\rangle$:

$$\Gamma(\vec{q}^{\,+}) = \sum_n \gamma_n(\vec{q}^{\,+}) |n\rangle\langle n| \tag{27}$$

with

$$\gamma_n(\vec{q}^{\,+}) \equiv \langle |x_n|^2 (1 - \tanh^2(\beta q^+ x_0)) \rangle_{\vec{\xi}} = \sum_\lambda \cos\left(\frac{2\pi n \lambda}{p} \right) \langle \xi_p \xi_\lambda (1 - \tanh^2(\beta q^+ x_0)) \rangle_{\vec{\xi}} \tag{28}$$

where $x_n \equiv \vec{\xi}|n\rangle$. Since $\Gamma(\vec{q}^{\,+})$ is symmetric, all the γ_ns will be real, as (28) shows explicitly. It can also be seen that, except in the case where $\beta \to \infty$, we have $0 < \gamma_n < c_n \forall n$.

This gives the following condition for $\vec{q}^{\,+}$ to be stable:

$$\max_n \left[\nu^2 + (1 - \nu)^2 + 2\nu(1 - \nu) \cos(2\pi n/p) \right]^{1/2} \gamma_n < T \,. \tag{29}$$

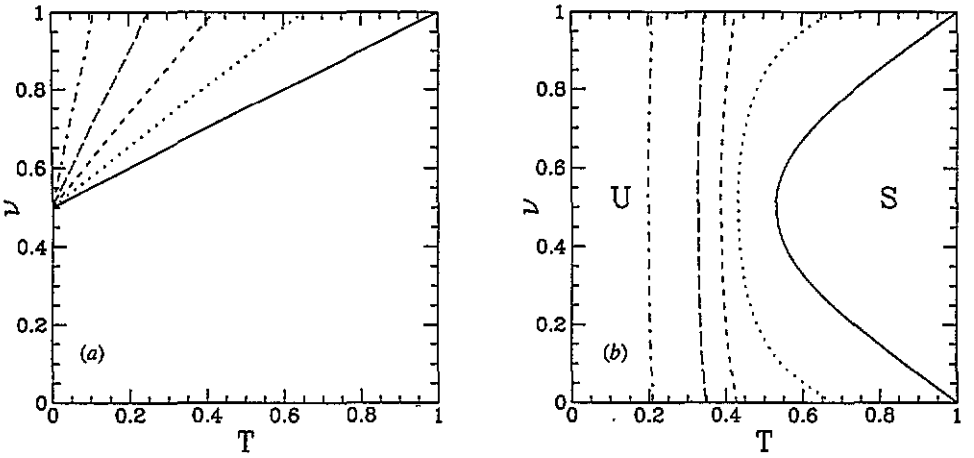

Figure 2. (*a*) The temperature $T_{\vec{q}^-}$ at which the pure antisymmetric fixed point $\vec{q} = q^-|p/2\rangle$ becomes a fixed point for the dynamics, for $p = 10$ and nearest-neighbour correlations of $c =$ 0 (full line), 0.2 (dotted line), 0.4 (short-broken line), 0.6 (long-broken line), 0.8 (chain line). (*b*) The temperature $T_{c'c}$, dividing parameter space into the corresponding regions in which the symmetric fixed point is stable (S) and unstable (U) under parallel dynamics.

This condition can be evaluated numerically, taking into account that the symmetric fixed point cannot become unstable due to fluctuations in the direction $n = 0$. We discover that the maximizing value of n under these conditions is $n = 1$, for the Ising-type correlations that we are using.

Bifurcation analysis for the symmetric fixed point gives the following condition for a continuous bifurcation to take place:

$$\gamma_n\left[\nu + (1-\nu)e^{2\pi i n/p}\right]\langle n|y\rangle = T\langle n|y\rangle\,. \tag{30}$$

As before, any bifurcation must take place in a direction $|n\rangle$, where a_n is real. For the case of the symmetric fixed point the bifurcation may not be in the direction $n = 0$. Therefore, if p is odd there will be no bifurcation. If p is even, a bifurcation can take place in the direction of the antisymmetric fixed point, $\vec{q} = \vec{q}^- = q^-|p/2\rangle$ at the temperature

$$T_b = \gamma_{p/2}(2\nu - 1)\,. \tag{31}$$

However, numerical evaluation of this temperature shows it to be always below the temperature at which the symmetric fixed point becomes unstable. This demonstrates that when this fixed point becomes unstable it will not go continuously to another fixed-point solution but will instead go to a limit cycle. We therefore identify as $T_{c'c}$ the temperature at which the symmetric fixed point becomes unstable, as given by the left-hand side of (29) with $n = 1$.

Finally, we attempt to locate T_{cr}. It is not possible to do this explicitly, but the analysis of CS suggests that, for p even, T_{cr} will be bounded from above by the temperature at which the pure antisymmetric state, $\vec{q}^-$, becomes a possible fixed point of the dynamics. This temperature is given by $T_{\vec{q}^-} = (2\nu - 1)c_{p/2}$. Since a recall state must have a non-zero overlap with the antisymmetric state $|p/2\rangle$, it makes sense that this temperature should form an upper bound on the temperature below which recall states are found.

If $\nu < 0.5$ we would expect to find period-p limit cycles below $T = (1 - 2\nu)c_{p/2}$.

We summarize the results of this section in figures 2(*a*) and (*b*), showing $T_{\vec{q}^-}$ and $T_{c'c}$, respectively.

3.3. Numerical results for $p = 10$, parallel dynamics

The dynamical laws described above, equation (3), were implemented numerically. These were not simulations on a finite-sized network but direct numerical iterations of the dynamics (3). Qualitatively, the phase diagram structure is as in figure 1, but with altered parameters.

To simplify the discussion of the results we describe the system in terms of three variables, Q_s, Q_d and the period P, where

$$Q_s(t) \equiv \frac{1}{p}\sum_{\mu} q_\mu(t) \qquad Q_d(t) \equiv |\vec{q}(t) - Q_s(t)\sqrt{p}|0\rangle| \tag{32}$$

and Q_s, Q_d denote the asymptotic values of these variables, $Q_s(\infty)$ and $Q_d(\infty)$. Along with the stability calculation of (29), these are all we need to determine the area of the phase diagram that the system is in, as follows:

- In the paramagnetic region P, Q_s and Q_d are both zero.
- In the symmetric fixed-point region S, Q_s is non-zero and Q_d is zero.
- In the limit-cycle regions C and C′, Q_d and P are non-zero. These regions are distinguished by the stability of the symmetric solution (calculated analytically in (29)).
- In the retrieval region R, the system is at a fixed point with $Q_d \neq 0$.
- In the period-p limit-cycle region R′, Q_d is non-zero and the period $P = p$.

The system was started in a 'pure state' ($q_\mu = 1, q_{\nu\neq\mu} = C_{\mu\nu}$) and run under the parallel dynamics (3). A small number of runs were undertaken from random starting positions. These seemed to confirm the result of CS that the asymptotic values of $|Q_s|$ and Q_d are independent of the initial q_μ's, indicating an attractor basin covering all random and pure start states for each value of the control parameters (p, ν, T). As in CS, these implementations do not distinguish between the C and C′ regions, but yield cyclical solutions in both cases from the above start states. The C and C′ regions are distinguishable by implementations started from a state close to the symmetric fixed point.

In all cases, the quantity used to measure the correlations was c, the correlation between neighbouring patterns in a sequence.

The results can be summarized as follows:

- The value of T_{cr} decreases rapidly with increasing c. The boundary between R, R′ and C is marked not just by an abrupt change in the period P, as would be expected, but also by an abrupt drop in the asymptotic value of Q_d.
- Within the C and C′ phases, as c increases at constant (ν, T), the asymptotic value of Q_d in general decreases. At low temperatures, however, after entering the phase, Q_d shows a slight increase with increasing c before abruptly dropping again. Any such sharp change in Q_d does not always correspond to changes in the period. If $T \lesssim 0.15$ then the period P changes slightly with increasing c, first increasing and then decreasing (for $\nu > 0.5$) or first decreasing and then increasing (for $\nu < 0.5$).
- Increasing c also decreases $T_{sc'}$. As T approaches $T_{sc'}$ from below, Q_d goes continuously to zero.
- Within the S phase, as T increases at constant (c, ν), Q_s goes continuously to zero.
- T_{ps} is confirmed as c_0.

Figure 3, showing asymptotic values of Q_d, P as a function of c for various values of T and $\nu = 0.2$, displays most of these features. There is a slight increase in Q_d as c is increased near $c \sim 0.3$, for $T = 0$. Inspection of the raw q_μ's shows that within this range the effect of increasing the correlation is to increase q_μ for the pattern with the

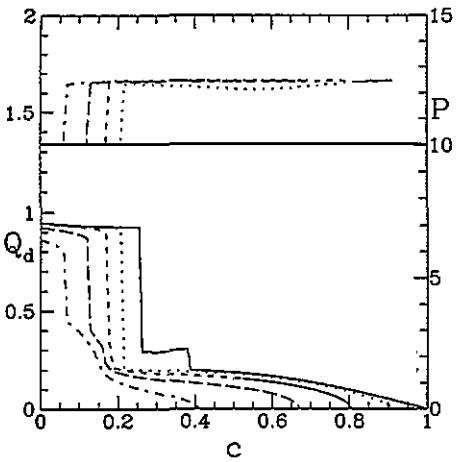

Figure 3. Q_d (lower curves, left-hand scale) and P (upper lines, right-hand scale), plotted against increasing c, for $p = 10$, $\nu = 0.2$, $T \in \{0$ (full curve), 0.1 (dotted curve), 0.2 (short-broken curve), 0.3 (long-broken curve), 0.4 (chain curve)$\}$. The system was started from a state of overlap 1 with one pattern and run under parallel dynamics. The sharp transition in Q_d and P marks the boundary of the R region.

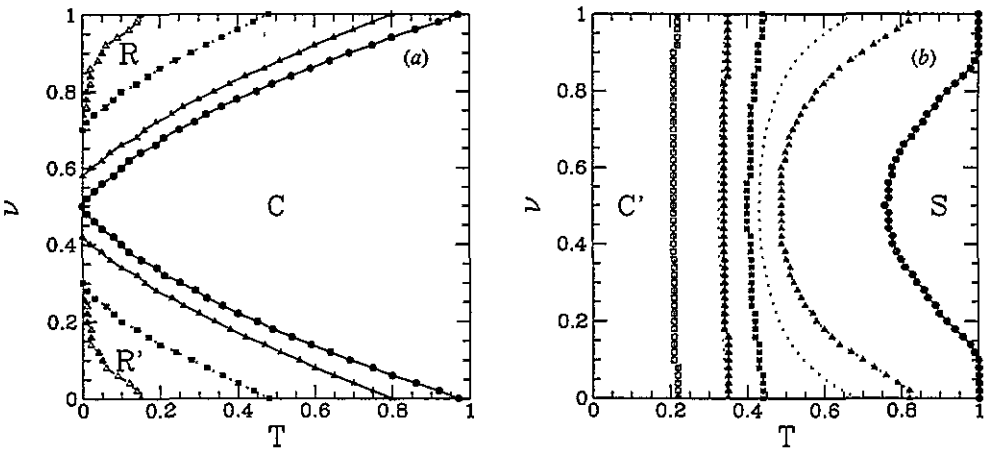

Figure 4. (*a*) T_{cr}, found numerically for parallel dynamics with $p = 10$ and $c = 0, 0.1, 0.2, 0.3$ (going from right to left). (*b*) $T_{sc'}$, found numerically for parallel dynamics with $p = 10$ and $c = 0, 0.2, 0.4, 0.6, 0.8$ (going from right to left). The dotted lines are the corresponding lines on which the symmetric fixed point becomes unstable for the same values of c, reproduced from figure 2(*b*) for ease of comparison.

second-highest overlap and decrease q_μ for the pattern with the second-lowest overlap. This will increase the standard deviation of the distribution of overlaps, which is exactly what Q_d measures. This increase in Q_d therefore does not correspond to the form of improved retrieval behaviour discussed in the introduction.

We conclude this section by presenting the values of $T_{sc'}$ and T_{cr} obtained by this numerical study (figures 4(*a*) and (*b*)). These are to be compared with the figures obtained analytically, figures 2(*a*) and (*b*). We obtain close agreement at high values of c between the boundary of the S phase and the stability of the symmetric fixed point, indicating that as correlations increase the size of the C′ region decreases rapidly. At lower values of c it is possible for limit-cycle behaviour to persist even when the symmetric fixed point is stable.

The upper bound obtained analytically for existence of the retrieval phase R can be seen to be extremely loose. In fact, we find numerically that there is no R or R′ phase at all for $c > 0.336$.

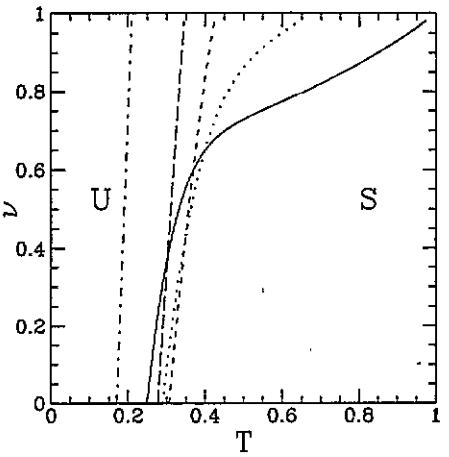

Figure 5. The regions in which the symmetric fixed point is stable (S) and unstable (U) under sequential dynamics for $p = 10$, with $c = 0$ (full curve), 0.2 (dotted curve), 0.4 (short-broken curve), 0.6 (long-broken curve), 0.8 (chain curve).

3.4. Sequential dynamics

As found by CS in the case of uncorrelated patterns, sequential dynamics can also lead to limit-cycle behaviour in the thermodynamic limit $N \to \infty$. However, numerical implementations of this system under sequential dynamics are far more expensive in terms of computer time than implementations of parallel dynamics. We therefore restrict this discussion to mentioning a few brief points of interest.

The symmetry between ν and $1 - \nu$ that exists for parallel dynamics does not exist for sequential dynamics. We therefore do not expect an R′ region of the phase diagram to exist.

The stability properties of the trivial fixed point are the same under both parallel and sequential dynamics.

The stability properties of the symmetric fixed point, however, show an interesting difference. We might expect that as c increases the temperature at which the symmetric fixed point becomes unstable would decrease monotonically, as for parallel dynamics. This is the case for p odd. For p even and low values of ν, on the other hand, as c is increased this critical temperature will first increase and then decrease. So there exists a small range of temperatures for which increasing the correlation will bring the system from the S phase to the C phase and then back to the S phase again. This is displayed in figure 5. Numerical implementations (starting from both the pure state and a state near the symmetric fixed point) confirm this result.

4. The double-propagating A-matrix

We now switch to look at the matrix $\mathbf{A}' \equiv \nu\mathbf{1} + \frac{1}{2}\sqrt{1-\nu^2}(\mathbf{S} - \mathbf{S}^\dagger)$, in the hope that the antisymmetric aspects of this matrix will reduce the strength of the symmetric fixed point in the case of correlated patterns. This matrix is very similar to that studied in [6, 7, 14]. These papers, however, looked at the case of very sparse coding so that no neuron was firing in more than one pattern. Here we are taking non-sparse coding ($\frac{1}{N}\sum_i \xi_i^\mu = 0 \forall \mu$) and a different form of correlations between patterns.

We expect the phases P, S, C and R to exist for $\mathbf{A}'$, as they existed for $\mathbf{A}$; however, we do not expect the boundaries to lie in the same positions, nor do we expect the detailed structure of the phase diagram necessarily to be the same. Since, for $\mathbf{A}'$, the $p = 2$ case gives the Hopfield network, it does not provide a useful toy model. Our ability to treat the model

analytically is therefore confined to calculating the stability of the trivial and symmetric fixed points and calculating the temperatures at which the symmetric and antisymmetric fixed points become solutions of the dynamics.

We confine our discussion to parallel dynamics for the reasons given in the previous section.

4.1. Analytic results for $p > 2$, parallel dynamics

The eigenvalues of $\mathbf{A}'$ with respect to the basis $|n\rangle$ are

$$\mathbf{A}'|n\rangle = a'_n|n\rangle \qquad a'_n = \nu + \mathrm{i}\sqrt{1-\nu^2}\sin\left(\frac{2\pi n}{p}\right). \tag{33}$$

We first attempt to discover the region in which the trivial fixed point will be the only attractor of the dynamics, using stability and bifurcation analysis. As before, a bifurcation from the trivial fixed point can only be in the direction of the symmetric or antisymmetric fixed point. The bifurcation temperatures are, respectively,

$$T_{\mathrm{bif}} = \nu c_0,\ \nu c_{p/2}\,. \tag{34}$$

These provide a lower bound on the paramagnetic phase.

Next we look at the stability properties of the trivial fixed point. Since $\Gamma(\vec{0}) = \mathbf{C}$, for stability of the trivial fixed point we require

$$\max_n |a'_n| c_n < T\,. \tag{35}$$

This leads to the following result:

- For $\nu < \nu_{\mathrm{crit}}(t_J) = \frac{1-t_J}{\sqrt{1+t_J{}^2}}$, the condition for stability is

$$T > T_{\mathrm{stab}} = \left[\frac{(1-t_J^p)(1-t_J^2)}{(1+t_J^p)(1+t_J{}^2-2t_Jk)}\right]\left[\nu^2+(1-\nu^2)[1-k^2]\right]^{1/2} \tag{36}$$

  where $k \equiv \cos\left(\frac{2\pi n}{p}\right) = \frac{2t_J}{(1-\nu^2)(1+t_J{}^2)}$, this gives the n that maximizes the LHS of the inequality (35).
- For $\nu > \nu_{\mathrm{crit}}$, the condition for stability is

$$T > c_0\nu \tag{37}$$

  and the maximizing value of n is 0, corresponding to an instability in the direction of the symmetric fixed point.

In the uncorrelated case, $\nu_{\mathrm{crit}} = 1$ and the trivial fixed point becomes unstable at $T = 1$ for parallel dynamics. The maximizing value of n will only be zero at $\nu = 1$. For any other value of ν the trivial fixed point becomes unstable in a direction other than the direction of the symmetric fixed point. In the correlated case, for $\nu > \nu_{\mathrm{crit}}$ the trivial fixed-point will go continuously to the symmetric fixed point as T is lowered. When $\nu < \nu_{\mathrm{crit}}$ the trivial fixed point becomes unstable in some other direction. The results of evaluating the above condition for $p = 10$ are shown in figure 6(a).

We now look at the stability properties of the symmetric fixed point. The condition (22) for stability results in the final condition

$$\max_{n\neq 0}\left[\nu^2+(1-\nu^2)\sin^2\left(\frac{2\pi n}{p}\right)\right]\gamma_n^2(\vec{q}^{\,+}) < T^2 \tag{38}$$

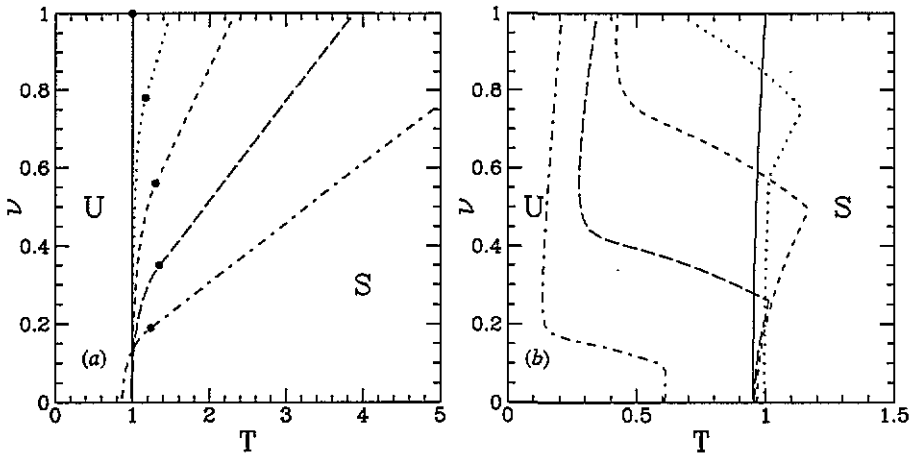

Figure 6. Regions where (*a*) the trivial fixed point and (*b*) the symmetric fixed point are stable (S) and unstable (U), found analytically for $p = 10$ under parallel dynamics, for $c = 0$ (full curve), 0.2 (dotted curve), 0.4 (short-broken curve), 0.6 (long-broken curve), 0.8 (chain curve). In (*a*), the full circles mark the point ($\nu_{\rm crit}$) where the trivial fixed point goes from becoming unstable in the direction of the symmetric fixed point (above the full circle) to becoming unstable in some other direction (below the full circle).

where

$$\gamma_n(\vec{q}^{\,+}) = \sum_\lambda \cos\left(\frac{2\pi n\lambda}{p}\right)\langle \xi_0\xi_\lambda(1-\tanh^2[\beta q^+\nu x_0])\rangle$$
$$q^+ = \langle x_0 \tanh[\beta\nu q^+ x_0]\rangle\,. \tag{39}$$

This too can be solved numerically and the results are displayed in figure 6(*b*). Interestingly, although the lines of stability for the symmetric and trivial fixed points coincide for some (low) values of ν and c, the point at which they separate is not the point at which the trivial fixed point becomes unstable in the direction of the symmetric fixed point. This implies that there is an area of the phase diagram in which the symmetric fixed point is a stable solution of the dynamics but the trivial fixed point will not become unstable in its direction, in contrast to the behaviour of the previous model.

Finally, we obtain an upper bound on the region in which recall behaviour is possible by calculating the temperature at which the antisymmetric fixed point becomes a possible fixed-point solution to the dynamics. This is found to be $\nu c_{p/2}$.

4.2. Numerical results for $p = 10$, parallel dynamics

We now present results obtained by numerical iteration of the macroscopic laws (3). As before, the behaviour of the network could be classified as R, C, S or P. As expected, we found no R′ region; there also proved to be no C′ region. The phase diagram is displayed below (figure 8). However, in this case the behaviour in the C region was strikingly different from the behaviour in the previous section. We first describe this behaviour and then describe the phase diagram.

- At low T there were multiple stable asymptotic values for Q_d (shown in figure 7(*a*)) when the system was started from random initial states. This contrasts with the previous case where the final values of Q_d, Q_s and P were independent of the initial states.

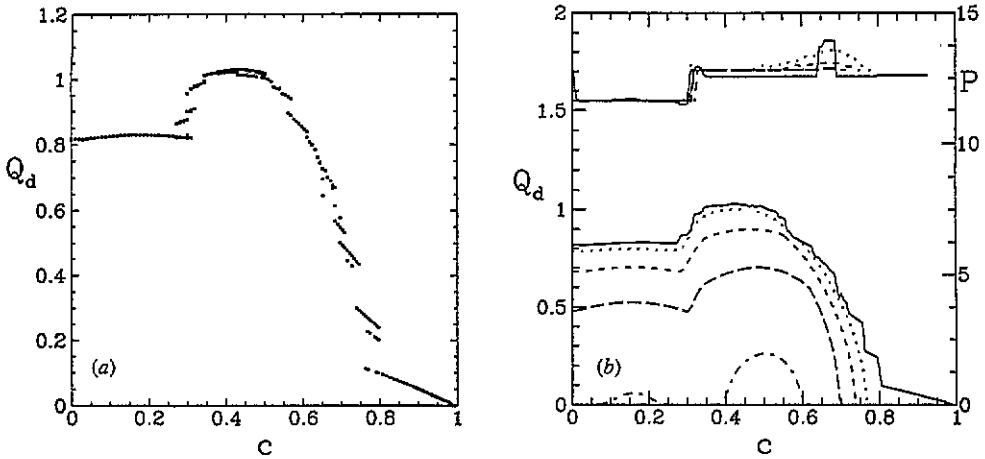

Figure 7. (*a*) Asymptotic values of Q_d for systems started from random states for $p = 10$, $\nu = 0.2$, $T = 0.01$. For $0.25 < c < 0.8$ there are, in general, multiple possible asymptotic values of Q_d. However, the tendency is for Q_d to increase with c until $c \sim 0.4$ and then decrease. (*b*) Q_d (lower curves) and P (upper curves) for $p = 10$, $\nu = 0.2$, $T = 0$ (full curve), 0.25 (dotted curve), 0.5 (short-broken curve), 0.75 (long-broken curve), 1 (chain curve). The curves for P are curtailed when $Q_d \to 0$ as then there is no periodic behaviour. The discontinuities in P for $T = 0$ are due to there being multiple asymptotic values of P; we were unable to find a way to ensure that the system ended up with one value rather than another. The curves displayed here were obtained by starting the system in the pure state; the results obtained by starting the system in random states display the same features.

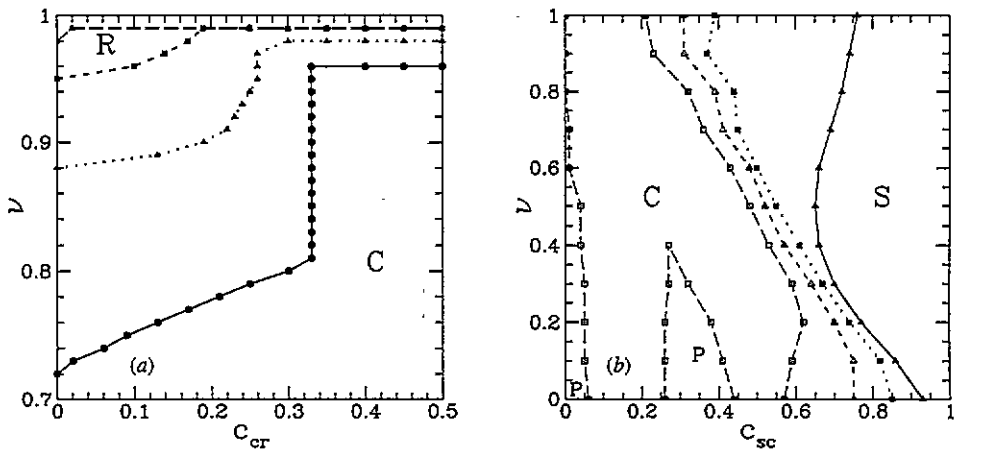

Figure 8. (*a*) The retrieval region R of the phase diagram for $p = 10$ and parallel dynamics. The curves of constant temperature divide the graph into the region where the pure state will go to a non-symmetric Hopfield-like fixed point (R) and the region where it will go to a limit cycle (C). The lines are at (going from C to R) $T = 0, 0.25, 0.5, 0.75$. (*b*) The limit-cycle region C for $p = 10$, shown as a function of (ν, c) for $T = 0.25, 0.5, 0.75, 1.0$. In the region S the system goes to the symmetric fixed point; in the region P, for $T = 1$, it goes to the trivial fixed point from a pure initial state. At $T = 0$ there is no S region; $c_{sc} = 1$.

As T increases, there is a decrease in the range of c for which this multiplicity of states exists, and a decrease in the number of states at any given c. Even at low T, as

figure 7(a) illustrates, this multiplicity of states does not prevent the emergence of the general trends, as follows.

- At fixed values of T and ν, increasing c no longer causes a monotonic decrease in Q_d. Instead, as c increases, Q_d initially increases too. At high values of T or low values of ν it peaks twice, with the second peak at a considerably higher value of Q_d than that obtained for $c = 0$, before decreasing (as we would expect) to 0. This behaviour is illustrated in figure 7(b), which also shows how this 'two-hump' effect is more pronounced at high T. The 'two-hump' effect is mirrored in the behaviour of the period P.
- The period displays an abrupt change in behaviour with increasing c. For $c < c_{\text{crit}}$, P is roughly constant. Above c_{crit}, P increases sharply and thereafter varies slightly with increasing c, first increasing and then decreasing.
  c_{crit} as defined here corresponds almost exactly to the value of c at which the minimal value of Q_d between the two humps first becomes 0. Around this value of c there is an oscillation in the envelope of the q_μ's as a function of time. At values of c much higher or lower than this, the envelope of the q_μ's is relatively constant with time.

We see that there are two separate limit-cycle solutions to the dynamics, one of which exists at high c and one of which exists at low c. The amplitudes of these solutions depend on c and T; at high T the ranges of c within which these amplitudes are non-zero and do not overlap, while at low T an overlap occurs, causing the oscillation in the envelope of the q_μ's with the corresponding beat frequency.

As stated in the introduction, the most interesting behaviour of the network is a stable cycle with a large amplitude of oscillation. The increase of Q_d with c prompts us to investigate whether increasing the correlations genuinely increases the extent to which the network distinguishes between patterns in the sequence. As was pointed out in the previous section, Q_d can be increased by increasing the span of the distribution of q_μ's, defined as $(\max_\mu q_\mu - \min_\mu q_\mu)$, but it can also be increased by increasing the tendency of the q_μ's to 'cluster' at their extreme values. If we look at the span as well as Q_d, we can say that for two distributions of q_μ with the same Q_d, the better performance is given by the system with a greater span. We do not display explicit results here for reasons of space, but the general findings are as follows.

For low c or low T, increasing c will not increase the span. If an increase in Q_d occurs it is therefore due to increased clustering. We also observe that at low c, Q_s is also small, implying that the q_μ's oscillate around 0 and that the system is not distinguishing between those patterns with large negative q_μ and those with large positive q_μ. For intermediate values of (ν, T, c), however, we find that an increase in Q_d is usually matched by an increase in the span. This is coupled with a non-zero value for Q_s. In practice, this means that we have limit-cycle behaviour in which one pattern has $q_\mu \sim 0.8$, another has $q_\mu \sim 0$, and the others are spread between them without too much clustering. In this region we can say that, paradoxically, the introduction of correlations genuinely causes the network to distinguish better between patterns.

We conclude by presenting the phase diagram for the network with $p = 10$. We do so in three parts. Figure 8(a) shows the border of the retrieval phase R as a function of c and ν for various values of T. As can be seen, for each value of T there is a ν at which c_{cr} increases abruptly. Above this ν we find there is no limit-cycle behaviour if the network is started in the pure state; this is a region of Hopfield-like behaviour.

Figure 8(b) shows the border of the limit-cycle region as a function of (c, ν) for various values of T. Figure 9 shows the region of stability of the symmetric fixed point as a function of (ν, T) for various values of c, for ease of comparison with figure 6(b). The agreement

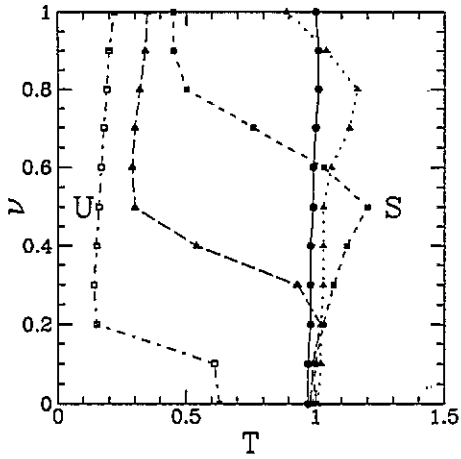

Figure 9. The regions in which the symmetric fixed-point is stable (S) and unstable (U), obtained numerically for $p = 10$ and shown as a function of (ν, T) for $c = 0$ (circles), 0.2 (full triangles), 0.4 (full squares), 0.6 (open triangles), 0.8 (open squares). This is to be compared with figure 6(*b*).

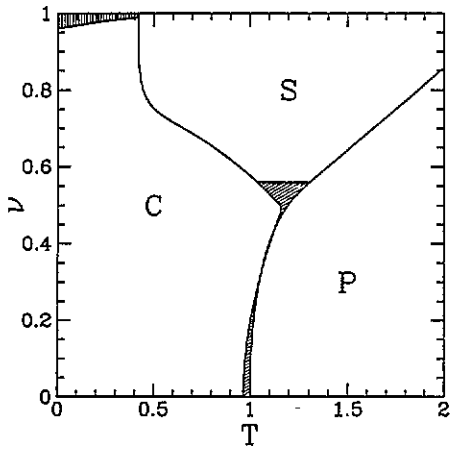

Figure 10. The phase diagram for the network for $p = 10$ and $c = 0.4$, showing the retrieval region R (vertical shading, in the top left-hand corner of the diagram), the limit-cycle region C, the region of coexistence of the symmetric fixed point and limit cycles C′ (diagonal shading, near $T = 1$), the symmetric fixed-point region S, and the paramagnetic region P.

between these two figures is good. Figure 10 is the overall phase diagram for the network with $c = 0.4$ and $p = 10$.

5. Conclusions

For a certain form of synaptic matrix in a neural network designed to store sequences of patterns, it is possible to improve limit-cycle behaviour by introducing moderate correlations between the stored patterns. The behaviour is improved in that the difference between the largest and smallest overlap with any pattern is increased; the value of the largest overlap is increased, and the absolute value of the smallest overlap is moved closer to 0, and the system distinguishes adequately between consecutive patterns in the sequence. This behaviour depends strongly on the structure of the synaptic matrix, and in the other case investigated the introduction of correlations served only to increase the tendency of the network to go to a state in which it does not distinguish between patterns at all.

The above comments apply to parallel dynamics, although the small amount of research done into sequential dynamics suggests that broadly the same results will be obtained in this case. The research has also been restricted to investigation of binary neuron neural networks, and to patterns with an overall magnetization of zero. We are still, therefore,

a long way from any kind of biological realism. One further step could be to attempt to determine the storage capacity for a network storing large numbers of finite-length sequences of patterns. This will be the subject of a future paper.

References

[1] Hopfield J J 1982 *Proc. Natl Acad. Sci., USA* **79** 2554
[2] Amit D J 1989 *Modelling Brain Function* (Cambridge: Cambridge University Press)
Muller B and Reinhardt J 1991 *Neural Networks: an Introduction* (Berlin: Springer)
[3] Kleinfeld D 1986 *Proc. Natl Acad. Sci., USA* **83** 9469
[4] Sompolinsky H and Kanter I 1986 *Phys. Rev. Lett.* **57** 2861
[5] Herz A V M, Li Z and van Hemmen J L 1991 *Phys. Rev. Lett.* **66** 1370
[6] Buhmann J and Schulten K 1987 *Europhys. Lett.* **4** 1205
[7] Nakamura T and Nishimori H 1991 *J. Phys. A: Math. Gen.* **23** 4627
[8] Coolen A C C and Sherrington D 1992 *J. Phys. A: Math. Gen.* **25** 5493
[9] Miyashita Y and Chang H S 1988 *Nature* **331** 68
[10] Miyashita Y and Chang H S 1988 *Nature* **335** 817
[11] Sakai K and Miyashita Y 1991 *Nature* **354** 152
[12] Griniasty M, Tsodyks M V and Amit D J 1993 *Neural Comput.* **5** 1
[13] A C C Coolen and T W Ruijgrok 1988 *Phys. Rev.* A **38** 4253
[14] Nishimori H, Nakamura T and Shiino M 1989 *Phys. Rev.* A **41** 3346